Europium(III) and terbium(III) *trans*-2-butenoates: syntheses, crystal structures, and properties

B. Barja [a], P. Aramendia [a], R. Baggio [b], M.T. Garland [c], O. Peña [d], Mireille Perec [a,*]

[a] *Departamento de Quimica Inorganica, Analitica y Quimica Fisica, Facultad de Ciencias Exactas y Naturales, INQUIMAE, Universidad de Buenos Aires, Ciudad Universitaria, Pabellon II, C1428EHA, Buenos Aires, Argentina*

[b] *Departamento de Fisica, Comision Nacional de Energia Atomica, Avda del Libertador 8250, 1429 Buenos Aires, Argentina*

[c] *Departamento de Fisica, Facultad de Ciencias Fisicas y Matematicas, Universidad de Chile, Avda Blanco Encalada 2008, Casilla 487-3, Santiago, Chile*

[d] *U.M.R. 6511, L.C.S.I.M. CNRS, Université Rennes I, 35042 Rennes, France*

Abstract

Homometallic europium(III) and terbium(III) *trans*-2-butenoate polymers, chemical formulas $[\{Eu_3(MeCH{=}CHCO_2)_9(H_2O)_4\}\cdot H_2O\cdot EtOH]_n$ (**1**) and $[\{Tb(MeCH{=}CHCO_2)_3(H_2O)\}\cdot MeCH{=}CHCO_2H]_n$ (**2**) and their dimeric 1,10-phenanthroline derivatives $[Ln_2(MeCH{=}CHCO_2)_6(phen)_2]\cdot 2H_2O$, with Ln = Eu (**3**) and Tb (**4**), were prepared and characterized by single-crystal X-ray diffraction. The coordination polymers **1** and **2** adopt different carboxylate-bridged infinite chain structures. While the europium compound **1** shows three independent europium centers linked to each other by three different types and number of carboxylate bridges, the terbium polymer **2** shows one independent metal center bridged by the same type of double carboxylates along the chains. Compounds **3** and **4** are isomorphous dinuclear structures with quadruply bridged carboxylate groups, two in the $\eta^1{:}\eta^1{:}\mu_2$ and two in the $\eta^2{:}\eta^1{:}\mu_2$ modes. The magnetic and photophysical behaviors of the four compounds are reported in the solid state.

Keywords: Crystal structures; Europium(III) complexes; Terbium(III) complexes; Luminescence

1. Introduction

The synthesis and physicochemical characterization of europium(III) and terbium(III) carboxylates is an area of current interest because of their potential applications in materials science, particularly in luminescent probes and sensory materials [1]. Previous reports on Eu(III) and Tb(III) multidentate aromatic carboxylates have shown an intriguing variety of microporous structures [2–5]. It may be noted, however, that structural studies on homometallic Eu(III) and Tb(III) compounds of aliphatic monocarboxylates as ligands, has been little explored. Reported cases involve the crystal structure of Eu(III) acetate $[Eu_2(CH_3CO_2)_6(H_2O)_4\cdot 4H_2O]$, which shows a dimeric unit with two acetate groups bridging two Eu(III) ions in *syn–syn* conformation [6], and the Tb(III) analogue is known to be isostructural [7]. Among higher homologues, only Tb(III) butyrate dihydrate was reported to crystallize in the monoclinic system, space group $P2_1/m$ ($Z = 4$) [8].

The lanthanide ion-size effects should be most significant in determining the structures of rare-earth monocarboxylates, due to likely steric constraints. It can, therefore, be expected that for a given carboxylate ligand, small variations in the lanthanide ionic radii may lead to a variety of new structures. Herein, we report the reactions leading to polymeric Eu(III) and Tb(III) *trans*-2-butenoates, $[\{Eu_3(MeCH{=}CHCO_2)_9(H_2O)_4\}\cdot H_2O\cdot EtOH]_n$ (**1**) and $[\{Tb(MeCH{=}CHCO_2)_3(H_2O)\}\cdot MeCH{=}CHCO_2H]_n$ (**2**) and to dimetallic $[Ln_2(MeCH{=}CHCO_2)_6(phen)_2]\cdot 2H_2O$, with Ln = Eu (**3**) and Tb (**4**) and phen = 1,10-phenanthroline. The results of this study include the X-ray structural determination of the four compounds and their magnetic and photophysical properties.

* Corresponding author. Tel.: +54-11-4576 3358; fax: +54-11-4576 3341.

E-mail address: perec@q1.fcen.uba.ar (M. Perec).

2. Experimental

2.1. Materials and methods

All starting materials were of AR grade and used without further purification. Elemental analyzes (C, H, N) were performed on a Carlo Erba EA 1108 instrument. Infrared spectra were recorded on a Nicolet FT IR 510 P spectrophotometer using the KBr pellet technique. Thermal analysis was performed on a Shimadzu DTG 50 thermal analyzer, under an air-flow of 40 l min^{-1} at a heating rate of 5 °C min^{-1}. Magnetic susceptibility was measured in the range 2–300 K, under an applied field of 5 k Oe (europium compounds) and 0.5 k Oe (terbium compounds) on a SHE-VTS 906 SQUID susceptometer. The magnetization data were corrected of the sample holder's contribution and the diamagnetic susceptibility of the core electrons, this latter calculated using Pascal's constants. The luminescence emission spectra of the compounds were recorded on a PTI QuantaMaster QM-1 luminescence spectrometer. Solid samples were placed between quartz plates and their luminescence was measured in a 30° front face geometry, detecting the emission from the back face. Excitation wavelength was 369 nm in all cases, and excitation and emission bandwidths were set to 4 and 2 nm, respectively. Luminescence lifetimes of the samples were measured in the same geometry as described for steady state spectra. The europium samples were excited at 532 and 354 nm, and the terbium ones at 354 nm with a frequency doubled or tripled Nd:YAG laser (Spectron), which delivered pulses of 8 ns FWHM at 10 Hz, 200 mJ at 532 nm, and 30 mJ at 354 nm. Emitted light passed through a monochromator and was detected with 4 nm bandwidth. Light was detected with a R928 Hamamatsu photomultiplier, amplified (SR.445, Stanford Research System) and the transient signal was averaged in a HP54502 digital oscilloscope and stored in a PC AT486. The traces were fitted to a single exponential decay and the goodness of the fit was judged by a homogeneous time-distribution of residuals.

2.2. Preparations

2.2.1. $[\{Eu_3(MeCH{=}CHCO_2)_9(H_2O)_4\}\cdot H_2O\cdot EtOH]_n$ (1)

Eu_2O_3 (0.35 g, 1 mmol) was added to a solution of *trans*-2-butenoic acid (0.70 g, 8.10 mmol) in a 1:1 water–ethanol solution (50 ml) was added. The reaction mixture was heated under reflux for 4 h under continuous stirring and filtered while hot. The clear solution was stored at room temperature (r.t.), and compound **1** was collected by filtration as a polycrystalline powder, washed with ethanol, and dried in air. Yield: (0.60 g, 70%). *Anal*. Calc. for $C_{38}H_{61}Eu_3O_{24}$: C, 33.60; H, 4.55. Found: C, 33.70; H, 4.60%. Main FT IR bands (KBr, cm^{-1}): 3424s,br $\nu_{(OH)}$, 1661vs $\nu_{(C=C)}$, 1530vs (ν_{CO_2asym}), 1451vs, 1426vs (ν_{CO_2sym}), 1290w, 1256m, 1105w, 970s, 918m, 748m, 700w, 536w, 420w. Thermogravimetric analysis shows that the first weight loss of 4.70% in the range 80–100 °C corresponds to simultaneous removal of the water and the ethanol solvate molecules. Subsequent thermal degradation occurs in several overlapping steps leading to the final residue at approximately 600 °C, which corresponds to the complete combustion of the compound to Eu_2O_3 as shown in the X-ray powder diffraction pattern [9].

2.2.2. $[\{Tb(MeCH{=}CHCO_2)_3(H_2O)\}\cdot MeCH{=}CHCO_2H]_n$ (2)

Terbium acetate tetrahydrate (0.34 g, 1 mmol) was added to a solution of *trans*-2-butenoic acid (0.43 g, 5 mmol) in water (10 ml). The solution was stirred at r.t. for 3 h, filtered off and left standing for a few weeks, whereupon colorless crystals of compound **2** were filtered off and dried in air. Yield: 0.30 g (60%). *Anal*. Calc. for $C_{16}H_{23}O_9Tb$: C, 37.05; H, 4.50. Found: C, 37.10; H, 4.40%. The IR spectrum was similar within $\pm$ 5 cm^{-1} to that described for **1** in the preceding paragraph.

2.2.3. $[Eu_2(MeCH{=}CHCO_2)_6(phen)_2]\cdot 2H_2O$ (3)

1,10-Phenanthroline monohydrate (0.40 g, 2.0 mmol) in methanol (30 ml) was added to a reaction mixture prepared as described for compound **1**. The solution was refluxed under stirring for 4 h, concentrated to 30 ml and passed through a glass filter. The filtrate was stored for a few days whereupon colorless crystals of compound **3** suitable for X-ray analysis were filtered off and dried in vacuum. The yield was about 70% based on the amount of Eu_2O_3 used. *Anal*. Calc. for $C_{24}H_{27}EuN_2O_8$: C, 46.20; H, 4.35; N, 4.50. Found: C, 46.30; H, 4.35; N, 4.60%. Main FT IR bands (KBr, cm^{-1}): 1659vs $\nu_{(C=C)}$, 1625m, 1578vs (ν_{CO_2asym}), 1541vs, 1451vs, 1430vs (ν_{CO_2sym}), 1352m, 1290w, 1252m, 1145w, 1102s, 968s, 912m, 864m (phen), 854m, 745m, 732m (phen), 723m, 696m, 544w, 513w, 417m.

2.2.4. $[Tb_2(MeCH{=}CHCO_2)_6(phen)_2]\cdot 2H_2O$ (4)

1,10-Phenanthroline monohydrate (0.40 g, 2.0 mmol) in methanol (30 ml) was added to a reaction mixture of terbium acetate tetrahydrate and *trans*-2-butenoate as described for compound **3**. The solution was refluxed under stirring for 4 h, concentrated to 30 ml and passed through a glass filter. The filtrate was stored for a few days whereupon colorless crystals suitable for X-ray analysis were filtered off and dried in vacuum. The yield was about 70% based on the amount of terbium acetate used. *Anal*. Calc. for $C_{24}H_{27}N_2O_8Tb$: C, 45.70; H, 4.30; N, 4.45. Found: C, 45.65; H, 4.30; N, 4.40%. The IR spectrum was similar within $\pm$5 cm^{-1} to that described for **3** in the preceding paragraph.

2.3. X-ray crystallography

Diffraction data were collected at r.t. on four circle Siemens R 3 m (**1** and **3**) or Bruker SMART 6000 CCD (**2** and **4**) diffractometers. All structures were primarily solved by direct methods using SHELXS-97 and completed through difference Fourier and refined by least-squares procedures on F_o^2 with SHELXL-97 [10]. Structures **1**, **3** and **4** present one disordered *trans*-2-butenoate each, which were modeled and refined split into two almost equipopulated sites. Hydrogens attached to non-disordered carbon atoms were positioned theoretically and allowed to ride. Terminal CH_3 groups were allowed to rotate as well. Hydrogens attached to oxygen in structures **1** and **2** were located in the late difference Fourier, and refined with restrained O–H and H···H distances. Those corresponding to the hydration water molecules in **3** and **4** were not found and consequently disregarded in the model. Crystal data collection and refinement parameters are given in Table 1.

3. Results and discussion

The reactions of europium(III) oxide and terbium(III) acetate with *trans*-2-butenoic acid in water and subsequent work-up led to the isolation of polymeric $[\{Eu_3(MeCH{=}CHCO_2)_9(H_2O)_4\}\cdot H_2O\cdot EtOH]_n$ (**1**) and $[\{Tb(MeCH{=}CHCO_2)_3(H_2O)\}\cdot MeCH{=}CHCO_2H]_n$ (**2**), respectively. When the medium contained excess 1,10-phenantholine the reactions under similar conditions afforded dimeric $[Eu_2(MeCH{=}CHCO_2)_6(phen)_2]\cdot 2H_2O$ (**3**) and $[Tb_2(MeCH{=}CHCO_2)_6(phen)_2]\cdot 2H_2O$ (**4**). The solid compounds are stable in dry atmosphere at room temperature. Single crystal X-ray analysis has been carried out on complexes **1**–**4** and crystallographic data are given in Table 1.

3.1. Crystal structures

Compound **1** crystallizes in the noncentrosymmetric space group *Pc* (no. 7), as polymeric chains running along *c*, the glide direction. The asymmetric unit contains three crystallographically different Eu centers coordinated to nine *trans*-2-butenoate anions and four aqua molecules, Fig. 1. A hydration water and an ethanol solvate molecules involved in hydrogen-bonding interactions, complete the structure. Selected bond lengths and Ln···Ln distances are listed in Table 2. In the asymmetric unit, Eu1 and Eu2 are surrounded by O_9 and Eu3 by an O_8 donor sets. Eu1 and Eu2 are bonded to eight carboxylate oxygen atoms and one oxygen water molecules. Eu1 is connected to the three bridging tridentate carboxylate oxygens O1A, O2A, O1D, O2D, O1H (one carboxylate oxygen is bound to two Eu atoms where the second is bound directly to one), two chelating carboxylate oxygens O1F, O2F, one bridging-bidentate carboxylate oxygen O1C and one water oxygen O3W in a tricapped trigonal-prismatic arrangement. Eu2 is connected to four bridging tridentate carboxylate oxygens O2B, O1D, O1H, O2H, O1I, O2I, one monodentate O1G, one bridging bidentate carboxylate oxygen O1E and O4W in a monocapped square-antiprism geometry. Eu3 is bonded to two water molecules and six carboxylate oxygens in a square-

Table 1
Crystal data and structural refinement parameters for **1**, **2**, **3** and **4**

	1	**2**	**3**	**4**
Chemical formula	$C_{38}H_{61}Eu_3O_{24}$	$C_{16}H_{23}O_9Tb$	$C_{24}H_{27}EuN_2O_8$	$C_{24}H_{27}N_2O_8Tb$
M	1357.75	518.26	623.44	630.40
Crystal system	monoclinic	triclinic	triclinic	triclinic
Space group	*Pc*, no. 7	$P\bar{1}$, no. 2	$P\bar{1}$, no. 2	$P\bar{1}$, no. 2
a (Å)	10.097(1)	7.895(1)	10.557(2)	10.538(1)
b (Å)	10.384(1)	10.780(1)	11.032(2)	11.010(1)
c (Å)	24.773(2)	13.575(1)	11.473(2)	11.429(1)
α (°)	90	97.00(1)	79.11(1)	78.89(1)
β (°)	96.35(1)	93.52(1)	71.54(1)	71.51(1)
γ (°)	90	107.34(1)	77.34(1)	77.25(1)
V (Å^3)	2581.4(5)	1088.7(1)	1226.2(3)	1215.8(2)
D_{calc} (g cm^{-3})	1.75	1.58	1.69	1.72
$F(000)$	1340	512	624	628
μ (mm^{-1})	3.68	3.29	2.61	2.96
R_1[a] $[F^2 > 2\sigma(F^2)]$	0.032	0.030	0.045	0.042
wR_2[b] $[F^2 > 2\sigma(F^2)]$	0.080	0.076	0.092	0.091
Max/min $\Delta\rho$ (e Å^{-3})	0.67, −0.84	1.04, −0.78	0.67, −0.75	0.75, −0.75

Features in common: $T = 23$ °C; $Z = 2$; crystal shapes: needles; color: colorless; absorption correction: semiempirical (ψ-scan).
[a] $R_1 = \Sigma||F_o| - |F_c||/\Sigma|F_o|$.
[b] $wR_2 = [\Sigma[w(F_o^2 - F_c^2)^2]/\Sigma[w(F_o^2)^2]]^{1/2}$.

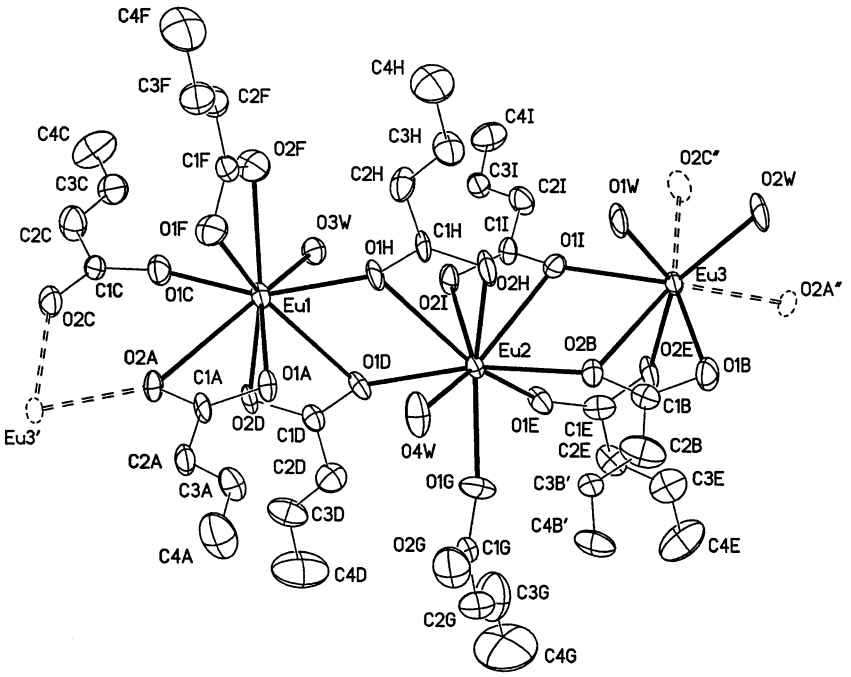

Fig. 1. Diagram (40% thermal ellipsoids) showing the asymmetric unit with atom labels of the linear chain in **1**. The disordered *trans*-2-butenoate B is represented by only one of the fragments.

antiprism geometry, four from tridentate carboxylate oxygens O2B, O1B, O1I, O2A and two bridging bidentate O2E, O2C. This complex coordination scheme gives rise to a linear array along c, where the cations Eu1, Eu2 and Eu3 are linked to each other by different types and number of bridges. Fig. 2 displays a schematic representation of the array of bridged europium cations along c in which the intrachain distances are: Eu1···Eu2 = 4.295(1) Å; Eu2···Eu3 = 4.148(1) Å and Eu1···Eu3 = 4.795(1) Å. The Eu–O distances vary in the range 2.278(8)–2.841(8) Å (average values: Eu1–O = 2.49(17), Eu2–O = 2.48(14) and Eu3–O = 2.43(10) Å).

The profuse availability of donors and acceptors for H-bonding results in a complex network summarized in Table 3. In terms of their effect they can be classified as "intra" or "inter" chain H-bonds. The former cooperate in the internal binding of the 1D polymer. Among the latter, only one bond contributes to the direct link between chains along the crystallographic a-direction, while all the rest organize into long chains of three or four steps (mediated by the solvates) and which link chains sideways in the transverse direction, the unique b-axis. Distances between chains along a and b are in the range of 10 Å. The space between chains is filled with interpenetrated *trans*-2-butenoate groups.

Compound **2** crystallizes in the centrosymmetric space group $P\bar{1}$ (no. 2), as polymeric chains built up by TbO_9 units along c. These are best described as tricapped trigonal-prisms with the Tb(III) ions coordinated to three bidentate *trans*-2-butenoates, one aqua molecule and two bonds from two short bridges provided by the centrosymmetric images of O2A and O1B. Besides, there is a non-coordinated *trans*-2-butenoic acid molecule stabilizing the structure, Fig. 3. There are two types of small loops, the "links" of the chain: Tb–O1B–Tb′–O1B′(–Tb) (′: $-1-x$, $1-y$, $-z$, Tb–Tb′:4.087 Å) and Tb–O2A–Tb″–O2A″(–Tb) (″: $-x$, $1-y$, $-z$, Tb–Tb″: 4.113 Å). The much simpler chain arising from

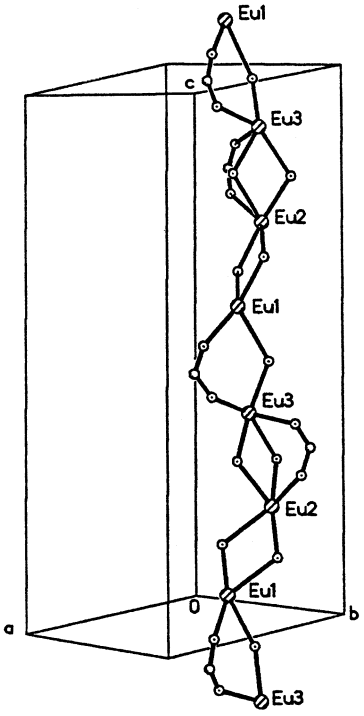

Fig. 2. Framework structure of **1** along the c-axis.

this scheme of terbium atoms is shown in Fig. 4. There are three strong H-bonds in the structure (Table 3 and Fig. 3). The one involving H1Wa provides to the intra-chain cohesion, while through the other two the *trans*-2-butenoic molecule binds to the polymeric structure.

Compounds **3** and **4** crystallize in the triclinic space group $P\bar{1}$ (no. 2); thus, we will restrict the structural presentation to the europium compound. Crystal data, and selected bond lengths and distances are presented in Tables 1 and 2, respectively. The structural unit is dimeric with an inversion center as shown in Fig. 5. Each Eu atom is coordinated to three *trans*-2-butenoates and one phenanthroline to give a nine-coordinateed Eu(III) center in a monocapped square-antiprism geometry. The EuO_7N_2 core comprises three carboxylate oxygen atoms from the tridentate carboxylate A, two from the bidentate carboxylate C, two from bridging bidentate carboxylates B and two N atoms from the chelating phenanthroline ligand.

Table 2
Selected bond lengths and distances (Å) for **1**, **2**, **3** and **4**[a]

1			
Eu(1)–O(1C)	2.278(8)	Eu(2)–O(4W)	2.488(9)
Eu(1)–O(1H)	2.398(8)	Eu(2)–O(1I)	2.661(9)
Eu(1)–O(3W)	2.408(8)	Eu(2)–O(1H)	2.751(9)
Eu(1)–O(1F)	2.423(9)	Eu(3)–O(1I)	2.371(9)
Eu(1)–O(1A)	2.429(9)	Eu(3)–O(2E)	2.384(9)
Eu(1)–O(2D)	2.461(9)	Eu(3)–O(1W)	2.417(9)
Eu(1)–O(2F)	2.474(10)	Eu(3)–O(2A)^{i}	2.433(7)
Eu(1)–O(1D)	2.698(9)	Eu(3)–O(1B)	2.437(10)
Eu(1)–O(2A)	2.841(8)	Eu(3)–O(2W)	2.448(9)
Eu(2)–O(1G)	2.312(10)	Eu(3)–O(2B)	2.648(8)
Eu(2)–O(2B)	2.386(9)	Eu(3)–C(1B)	2.926(10)
Eu(2)–O(1D)	2.397(8)	Eu(1)···Eu(2)	4.2941(9)
Eu(2)–O(1E)	2.419(8)	Eu(2)···Eu(3)	4.1476(8)
Eu(2)–O(2H)	2.454(9)	Eu(3)···Eu(1)^{i}	4.7949(8)
Eu(2)–O(2I)	2.455(10)		
2			
Tb–O(2^{a})^{ii}	2.338(2)	Tb–O(1C)	2.481(3)
Tb–O(1B)^{iii}	2.353(2)	Tb–O(1B)	2.551(2)
Tb–O(1W)	2.387(3)	Tb–O(2A)	2.573(2)
Tb–O(2C)	2.393(3)	Tb···Tb^{iii}	4.087(1)
Tb–O(1^{a})	2.403(3)	Tb···Tb^{ii}	4.113(1)
Tb–O(2B)	2.433(3)		
3			
Eu–O(1B)^{iv}	2.358(5)	Eu–O(1C)	2.495(6)
Eu–O(1^{a})^{iv}	2.368(5)	Eu–N(1)	2.598(6)
Eu–O(2B)	2.374(5)	Eu–O(1A)	2.599(5)
Eu–O(2^{a})	2.466(5)	Eu–N(2)	2.615(6)
Eu–O(2C)	2.473(6)	Eu···Eu^{iv}	3.935(1)
4			
Tb–O(2^{a})^{v}	2.332(4)	Tb–O(2C″)	2.502(11)
Tb–O(2B)^{v}	2.336(4)	Tb–O(2C′)	2.497(9)
Tb–O(1^{a})	2.346(4)	Tb–O(2B)	2.580(4)
Tb–O(1B)	2.424(4)	Tb–N(2)	2.585(5)
Tb–O(1C′)	2.441(9)	Tb–N(1)	2.581(4)
Tb–O(1C″)	2.495(11)	Tb···Tb^{v}	3.911(1)

[a] Symmetry codes: (i) $x, 2-y, 0.5+z$; (ii) $-x, 1-y, -z$; (iii) $-1-x, 1-y, -z$; (iv) $2-x, -5, 2-z$; (v) $1-x, 1-y, 1-z$.

It is interesting to note that the discrete dinuclear unit shows fourfold bridging between the metal centers, two long bridges of the bidentate bridging type (Eu–O1B–C1B–O2B–Eu′, ′: $2-x, -y, 2-z$) and two short bridges by monoatomic O atoms (Eu–O1A–Eu′). The Eu···Eu′ distance of 3.935(1) Å is slightly larger than the Tb···Tb′ distance of 3.911(1) Å, likely as a result of its position in the lanthanide series (ionic radii 0.95 Eu(III) vs. 0.92 Tb(III) Å). The structure is completed by two hydration water molecules, one of which appears depleted with an occupation factor of approximately 0.60. No hydrogen atoms could be found on these water molecules, but the presence of hydrogen bonds can be inferred from the rather short distances between these water oxygen atoms and the carboxylate oxygens of the disordered *trans*-2-butenoate C (2.80–2.90 Å). These hydrogen bonds may link adjacent dimers along the *c*-direction giving rise to H-bonded "chains". Interactions in other directions appear to be of the van der Waals type.

3.2. Magnetic properties

The temperature dependences of the molar magnetic susceptibility of the europium-based compounds **1** and **3** are shown in Fig. 6. The overall behavior of the susceptibility can be described by a non-zero value at room temperature and an almost linear increase with decreasing temperature followed by a plateau between

Table 3
H-bonding interactions in **1** and **2**[a]

	D–H (Å)	H···A (Å)	D···A (Å)	<(DHA) (°)
1				
O1X–H1X···O5W	0.90(2)	2.00(2)	2.601(17)	123(3)
O1W–H1WA···O1X	0.90(2)	1.87(3)	2.766(14)	174(6)
O1W–H1WB···O2H	0.90(2)	1.89(8)	2.633(11)	138(10)
O2W–H2WA···O2D^{i}	0.90(2)	1.77(3)	2.650(11)	166(10)
O2W–H2WB···O1X	0.90(2)	1.91(3)	2.806(15)	172(7)
O3W–H3WA···O2I	0.88(2)	1.90(3)	2.721(12)	156(3)
O3W–H3WB···O2G^{ii}	0.89(2)	1.99(7)	2.746(15)	142(10)
O4W–H4WA···O2G	0.90(2)	2.19(5)	3.000(20)	150(7)
O4W–H4WB···O1A	0.90(2)	1.97(3)	2.856(13)	170(9)
O5W–H5WA···O2E^{iii}	0.93(4)	2.02(3)	2.871(15)	150(10)
O5W–H5WB···O1F^{iv}	0.90(3)	1.99(2)	2.674(15)	131(5)
2				
O1W–H1WA···O2B^{v}	0.7431)	2.03(2)	2.754(4)	164(6)
O1W–H1WB···O1D	0.83(4)	1.86(5)	2.687(6)	172(5)
O2D–H2D···O1C	1.08(9)	1.66(9)	2.608(7)	143(7)

[a] Symmetry codes: (i) $x, 2-y, 0.5+z$; (ii) $1+x, y, z$; (iii) $x, 1+y, z$; (iv) $x, 3-y, 0.5+z$; (v) $-x, 1-y, -z$.

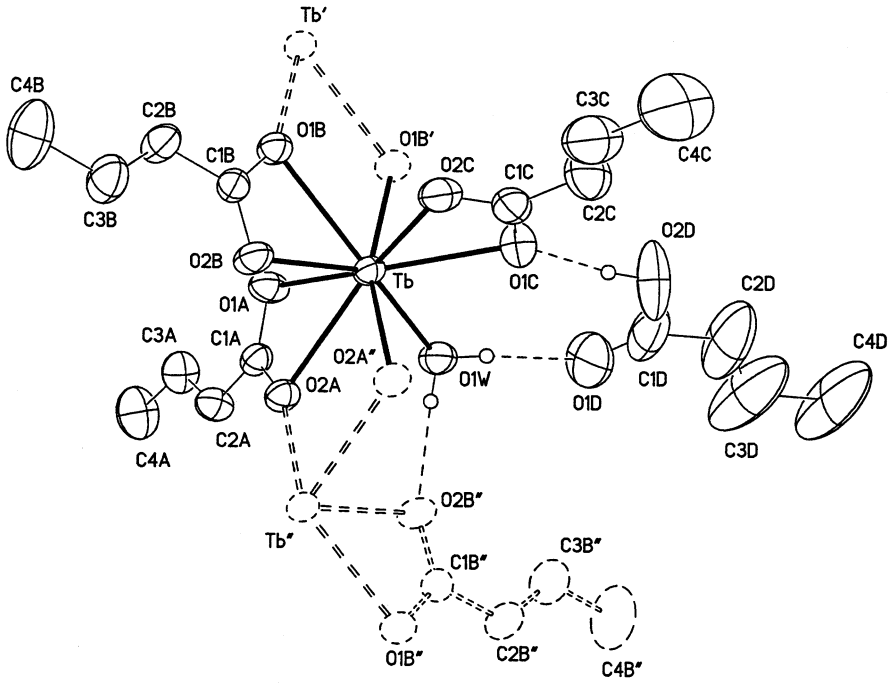

Fig. 3. Diagram (40% thermal ellipsoids) showing the asymmetric unit with atom labels of the linear chain in **2**.

50 and 100 K; at lower temperature, a sample-dependent increase is observed. The experimental magnetic moment at room-temperature, $\mu = \sqrt{8.\chi.T}$, is about 3.2 μ_B, suggesting a van Vleck contribution due the admixture between the $^7F_0$ and $^7F_1$ states, which leads to a non-negligible moment, 3.6 μ_B or more according to the literature, at intermediate and high temperatures [11,12]. The thermal depopulation of the excited $^7F_1$ state with decreasing temperature explains the linear increase of the magnetic susceptibility between room temperature and 110–120 K. The plateau value, or van Vleck susceptibility, attained at about 100 K is quite similar for both compounds, and should be related to the energy difference between the $J = 0$ and $J = 1$ states. At lower temperatures, a Curie term is superposed to the van Vleck susceptibility, leading to a quite negligible contribution of the magnetization for compound **1** and to a more significant contribution for compound **3**. The profiles of the curves did not change significantly after recrystallization and we attribute the magnetic term in **3** to small amounts of paramagnetic impurities.

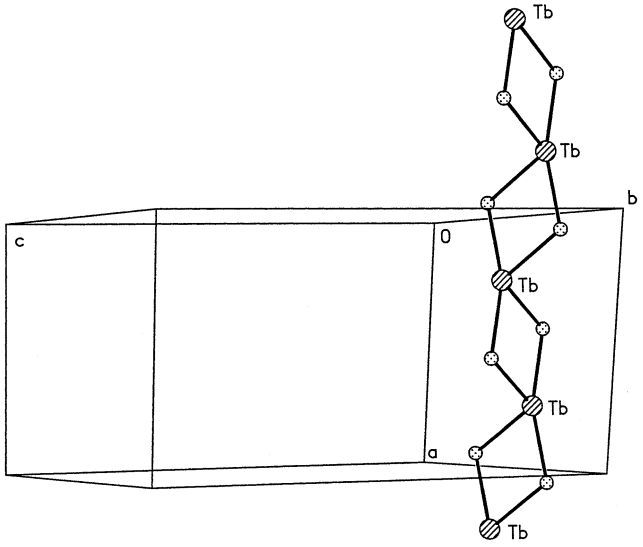

Fig. 4. Framework structure of **2** along the c-axis.

The temperature dependencies of the inverse of the molar susceptibility of the terbium-based compounds **2** and **4** follow a Curie (or Curie–Weiss) law, with almost perfect linearity in the whole temperature range (not shown). The observed effective magnetic moments of 9.57 μ_B in both cases are in good agreement with the theoretically expected value of 9.72 μ_B for a Tb(III) free-ion, while the Curie–Weiss temperature θ is approximately zero within experimental errors (-0.1 and -0.4 K, for **2** and **4**, respectively).

3.3. Luminescent properties

Fig. 7 shows the luminescence excitation and emission spectra of microcrystalline powder samples of **1** and **3**, respectively. Those of samples **2** and **4** are very similar and, therefore, are not shown in the Figure. In the emission spectra, the characteristic Eu(III) metal centered transition bands ($^5D_0 \rightarrow {}^7F_J$) for $J = 1$, 2 and 4 are observed at approximately 590, 615 and 695 nm, respectively. For the terbium compounds, the metal centered transition bands ($^5D_4 \rightarrow {}^7F_J$) for $J = 6$, 5, 4 and 3 are observed at 489, 544, 584 and 621 nm, respectively. In compounds **3** and **4**, the phenanthroline ligand acts as

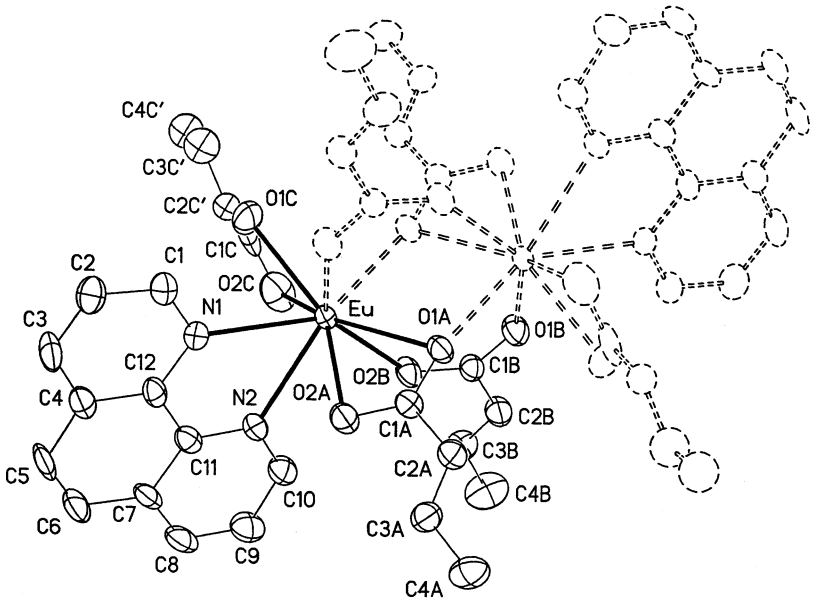

Fig. 5. Molecular structure (40% thermal ellipsoids) of $[Eu_2(MeCH{=}CHCO_2)_6(phen)_2]\cdot 2H_2O$ (**3**). The disordered *trans*-2-butenoate C has been represented by the fragment with larger occupation.

an antenna, which absorbs the excitation light of 350 nm and transfers it to the emissive state of the metal. Thus, the intensity of their luminescence becomes markedly enhanced when compared with those of **1** and **2.** In Fig. 7(right), the excitation spectrum shows the bands of Eu(III) (mainly at 394 nm) and the very strong band of phenenthroline at wavelengths lower than 350 nm.

The emission decays of **1**–**4** could be well described by a monoexponential curve. The values of the emission decay times in ms were 0.37 ($\lambda_{exc} = 532$ nm), 1.35 ($\lambda_{exc} = 354$ nm), 1.1 ($\lambda_{exc} = 354$ nm) and 0.15 ($\lambda_{exc} = 354$ nm), respectively, for compounds. It is known that the vibronic coupling between the excited states of the lanthanide ions and the OH oscillators of coordinated water molecules provides an efficient path for the radiationless deactivation of electronic energy.

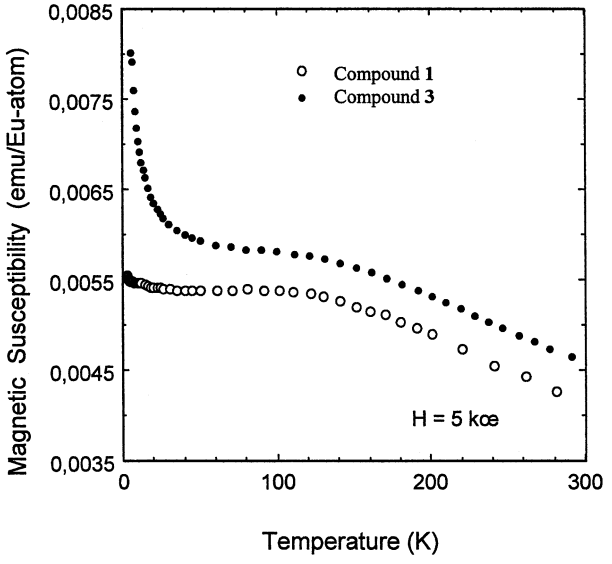

Fig. 6. Molar susceptibility vs. temperature for the europium compounds **1** and **3**.

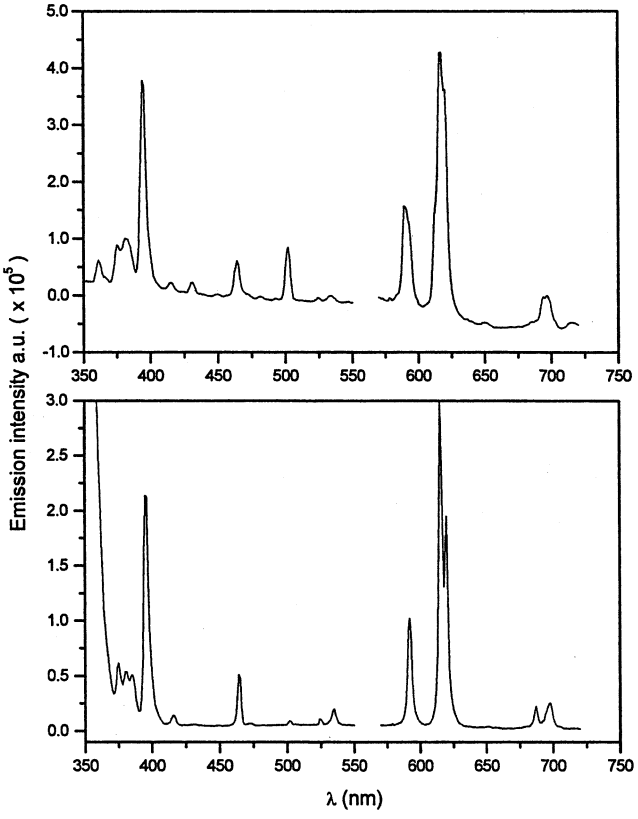

Fig. 7. Excitation ($\lambda_{em} = 615$ nm) and emission spectra ($\lambda_{exc} = 394$ nm) of europium solid samples. Compounds **1** ($\lambda_{exc} = 394$ nm) upper panel and compound **3** ($\lambda_{exc} = 350$ nm) lower panel.

Although the emission decay times of compounds **1**, **2**, and **3** evidence the sensitivity of the excited state to the number of coordinated water molecules, compound **4** does not follow the same trend, showing the shortest value even when no water molecules are directly bound to the Tb(III) ion. This can be explained in terms of the difference in energy between the excited energy levels of the phenanthroline and the Eu(III) and Tb(III) in **3** and **4**, respectively. For phenanthroline, the formation of the first excited singlet state by absorption is followed by the population of the triplet state by intersystem crossing with an efficiency close to unity [13]. Then, the energy is transferred to the excited metal-centered levels from which the deactivation occurs via radiative and non-radiative paths. In principle, the efficiency of the ligand-to-metal energy transfer process should be favored by a matching of the energy levels of the donor and the acceptor, being the energy levels of the donor higher than those of the acceptor. However, if this difference in energy is too small, thermally activated back energy transfer can occur, affecting both the intensities and lifetimes of the emission [14]. In compound **3**, the energy gap between the triplet state of the phenanthroline (22 100 cm^{-1}) [15] and the emissive $^5D_0$ level of Eu(III) (at 579 nm in Fig. 1) is 4829 cm^{-1} while that of Tb(III) in **4** is only 1650 cm^{-1} ($^5D_4$ at 489 nm) giving rise to a back energy transfer process from Tb(III) to the ligand. In fact, this back energy transfer mechanism would depopulate the emissive $^5D_4$ level of Tb(III) with the consequent reduction of the lifetime of the emission. Similar results were described for some other Tb(III) chelates involving macrocyclic ligands [15,16].

4. Conclusions

The aliphatic monocarboxylate *trans*-2-butenoate ligand reacts with Eu(III) and Tb(III) ions to give interesting polymeric compounds **1** and **2**, with a variety of doubly and triply carboxylate bridges between the metal centers. Addition of phen to the reacting mixtures leads to the isomorphous quadruply bridged dimers $[Ln_2(trans\text{-}2\text{-butenoate})_6(phen)_2]\cdot 2H_2O$ with Ln = Eu **3** and Tb **4**, with two carboxylates in the $\eta^1{:}\eta^1{:}\mu_2$ two in the $\eta^2{:}\eta^1{:}\mu_2$ bridging modes. The emission spectra studies show a relatively short lifetime of the $^5D_4$(Tb) state of **4**, which is attributed to back energy transfer to phenanthroline excited states competing with metal centered luminescence.

5. Supplementary material

Crystallographic data for the structures reported in this paper have been deposited with the Cambridge Crystallographic Data Center as supplementary publication #CCDC-200203 (**1**),CCDC-200204 (**2**), CCDC-200205(**3**) and CCDC-200206(**4**). Copies of the data can be obtained free of charge on application to The Director, CCDC, 12 Union Road, Cambridge, CB2 1EZ, UK (fax: +44-1223-336-033; e-mail: deposit@ccdc.cam.ac.uk or www: http://www.ccdc.cam.ac.uk).

Acknowledgements

This work was supported by Fundacion Andes C-13575, CONICYT FONDAP 11980002, PICS 922, FONDECYT 1020802 (Chile) and ANPCyT PICT 4438 and CONICET-PIP 0388 (Argentina). P.F.A. and M.P. are members of CONICET.

References

[1] (a) J.-C.G. Bünzli, in: J.-C.G. Bünzli, G.R. Choppin (Eds.), Lanthanide Probes in Life, Chemical and Earth Sciences, Theory and Practice, Elsevier, Amsterdam, 1989, p. 219;
(b) A.P. de Silva, H.Q.N. Gunaratne, T.E. Rice, Angew. Chem., Int. Ed. Engl. 35 (1996) 2116;
(c) A. Mortellaro, D.G. Nocera, J. Am. Chem. Soc. 118 (1996) 7414.
[2] L. Ma, O.R. Evans, B.M. Foxman, W. Lin, Inorg. Chem. 38 (1999) 5837.
[3] C. Seward, N.-X. Hu, S. Wag, J. Chem. Soc., Dalton Trans. (2000) 134.
[4] C.-D. Wu, C.-Z. Lu, W.-B. Yang, S.-F. Lu, H.-H. Zhuang, J.-S. Huang, Eur. J. Inorg. Chem. (2002) 797.
[5] T.M. Reineke, M. Eddaoudi, M. Fehr, D. Kelley, O.M. Yaghi, J. Am. Chem. Soc. 121 (1999) 1651.
[6] Y. Yansheng, L. Lubin, T.C.W. Mak, Chin. J. Struct. Chem. (Jiegou Huaxue) 7 (1988) 1.
[7] Gmelin Handbook of Inorganic Chemistry, Sc, Y, La–Lu, Carboxylates, D5, 1984.
[8] M.A. Nabar, S.D. Barve, J. Appl. Crystallogr. 17 (1984) 39; Chem. Abstr. 100, 59895g.
[9] The diffraction pattern was matched with that of Eu_2O_3: The JCPDS International Center for Diffraction Data, Swarthmore, PA, 1992, Powder Diffraction File No.340072.
[10] G.M. Sheldrick, SHELXS-97 and SHELXL-97, Software for Crystal Structure Analysis, Siemens Analytical X-ray Instruments, Madison, WI, 1997.
[11] J.H. Van Vleck, The Theory of Electric and Magnetic Susceptibilities, Oxford University Press, London, 1965.
[12] A. Herpin, Theorie de Magnetisme, Presses Universitaires de France, Paris, 1968.
[13] S.L. Murov, I. Carmichael, G. Hug, Handbook of Photochemistry, Marcel Dekker, New York, 1993, p. 37.
[14] (a) D. Parker, J.A. Gareth Williams, J. Chem. Soc., Dalton Trans. (1996) 3613.;
(b) D. Parker, R.S. Dickins, H. Puschmann, C. Crossland, J.A.K. Howard, Chem. Rev. 102 (2002) 1977.
[15] S. Quici, G. Marzanni, M. Cavazzini, P.L. Anelli, M. Botta, E. Gianolio, G. Accorsi, N. Armaroli, F. Barigelletti, Inorg. Chem. 41 (2002) 2777.
[16] B. Alpha, R. Ballardini, V. Balzani, J.M. Lehn, S. Perathoner, N. Sabbatini, Photochem. Photobiol. 52 (1990) 299.